

Remote Photocatalytic Activity as Probed by Measuring the Degradation of Self-Assembled Monolayers Anchored near Microdomains of Titanium Dioxide

Hossam Haick and Yaron Paz*

Department of Chemical Engineering, Technion-Israel Institute of Technology, Haifa 32000, Israel

Received: October 13, 2000; In Final Form: December 12, 2000

A cross-linked self-assembled monolayer (SAM) of octadecyltrichlorosilane (OTS) was chemisorbed on well-defined structures, comprised of alternating microstripes of TiO_2 and silicon. The kinetics of the photodegradation of the anchored SAM on the hybrid structure was then measured in situ by FTIR under controlled humidity and surface temperature. It was found that mineralization of the aliphatic chains anchored to the inert silicon domains can occur, even when these chains are located as far as $20\ \mu\text{m}$ away from the photocatalytic titanium dioxide microdomains. An apparent first-order kinetics was found for each of the two domain types. Apparent activation energies were calculated on the basis of the temperature-dependent measurements. The observation that the oxidizing species can induce mineralization far from the locus of their formation may have large effect on the design and modeling of porous photocatalysts having “dark” pores and on the developing of hybrid photocatalysts.

1. Introduction

Titanium dioxide is a well-known photocatalyst for water and air treatment.¹ The general scheme for the photocatalytic destruction of organics begins with the excitation of the semiconductor following illumination with supra-band-gap photons. The electron–hole pairs migrate to the surface of the photocatalyst, where the holes may be trapped by H_2O or OH^- adsorbed at the surface, thus forming highly reactive hydroxyl radicals. Similarly, the electrons may be trapped in oxygen vacancies deep traps or in shallow traps on surface sites.^{2,3} On the basis of the Langmuir–Hinshelwood type of kinetics, observed in the liquid phase⁴ or in the gas phase,⁵ it is commonly taken that the hydroxyl radicals do not leave the titanium dioxide surface; hence, adsorption of the contaminant on the photocatalyst is a prerequisite for the photodegradation to occur.

Structures comprised of photoactive titanium dioxide and inert adsorbents may enhance the overall performance of the photocatalyst by concentrating molecules, which do not adsorb on TiO_2 , at the vicinity of the photocatalyst. A few examples are the degradation of Rhodamine 6G in solutions containing particles comprised of $\text{SiO}_2\text{--TiO}_2$ ⁶ or the photodegradation of propionaldehyde by particles comprised of adsorptive sites (activated carbon, zeolites, etc.) located at the vicinity of photocatalytic sites.⁷ Here, the net increase in the photodegradation rate was explained in most cases as being due to surface diffusion of the contaminants and not as due to diffusion of the hydroxyl radicals from the TiO_2 sites, where they are formed, to the adsorptive sites.

In this paper, a method for the observation of out-diffusion of active species is presented, demonstrating that the oxidizing species formed on the titanium dioxide surface are capable of surface migrating as far as $20\ \mu\text{m}$ away. The method is based on an FTIR study of the photocatalytic degradation of self-assembled monolayers anchored on well-defined hybrid structures consisting of inert microdomains of silicon and photocatalytic microdomains of titanium dioxide.

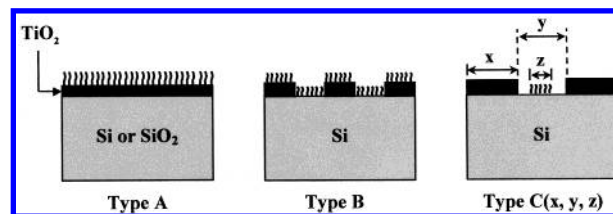


Figure 1. The three types of samples that were used.

2. Experimental and Methods Section

2.a. Sample Preparation and Characterization. Three types of samples were prepared (Figure 1): *A-Type Samples.* A-type samples are nonpatterned TiO_2 -coated silicon wafers, covered with monolayers of octadecyltrichlorosilane (OTS). The preparation of the A-type samples included the coating of a set of 1 in. silicon wafers (P-type (111), polished on both sides, 3000 $\Omega\text{-cm}$, Topsil, Frederikssund, Denmark) by a thin (70 nm), well-adhered, nanocrystalline TiO_2 (anatase) film, produced by a sol-gel process, similar to the one used by us for the preparation of self-cleaning glass^{8,9} but with a calcination temperature of 450 $^\circ\text{C}$. Cross-linked self-assembled monolayers (SAMs) of octadecyltrichlorosilane (OTS, $\text{CH}_3(\text{CH}_2)_{17}\text{SiCl}_3$) were then chemisorbed by the self-assembly method.¹⁰ These monolayers are known to consist of long alkyl chains attached covalently to the surface of oxides by siloxane bonds (Si--O--Si for a silicon oxide substrate, Si--O--Ti for a titanium dioxide substrate), where adjacent chains are cross-linked by Si--O--Si bonds. Due to these strong covalent bonds and due to the close packing of the chains, these molecular arrays are very robust and can withstand temperatures as high as 180 $^\circ\text{C}$.¹¹

The C–H stretch envelope (i.e. $\text{CH}_2(\text{a})$, $\text{CH}_2(\text{s})$, $\text{CH}_3(\text{a})$, $\text{CH}_3(\text{s})$) of the Fourier transformed infrared spectra (FTIR, Bruker IFS55, measured with 4 cm^{-1} resolution) of these samples was measured and integrated. On the basis of the integrated values, a ratio of 4:1 between the signal of OTS anchored to A-type samples and OTS anchored to silicon was obtained. Taking into account that the average distance between nearest chains is governed mainly by the Si--O--Si bond length that should not differ by much in the two substrates, it is

* Corresponding author. Tel: +972-4-8292486. Fax: +972-4-8230476. E-mail: paz@tx.technion.ac.il.

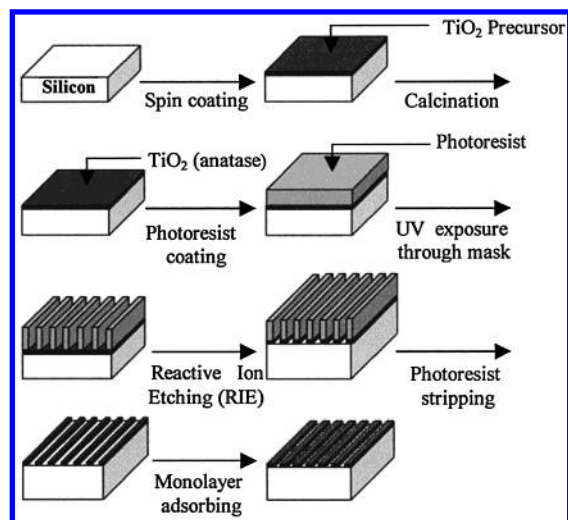


Figure 2. Preparation scheme of B-type samples.

reasonable to assume that the difference in the OTS coverage was mainly due to the larger actual surface area of the spin-coated titanium dioxide film.¹²

Some experiments were done with samples made of the same titanium dioxide layer, coated on fused silica instead of silicon wafers. These samples are denoted in this manuscript as A2-type samples.

B-Type Samples. B-type samples consisted of OTS monolayers, chemisorbed on substrates made of alternating, repetitive microstrips of silicon and titanium dioxide. The preparation of these samples included the following steps (Figure 2):¹²

(i) coating of a silicon wafer with the same titanium dioxide film used for A-type samples;

(ii) spin-coating the TiO₂ layer with a positive photoresist (AZ1818, Shipley) and then prebaking (90 °C, 10 min.);

(iii) exposure through a specific mask. (for this stage, preparation of a set of masks, each consisting of alternating stripes of equal width and distance, with widths of 2.5, 5, 10, and 40 μm);

(iv) developing (DEV326, Shipley) and postbaking, leaving a structure made of protected and unprotected stripes, having predetermined width;

(v) etching of the unprotected titanium dioxide domains, to the silicon substrate, by reactive ion etching (RIE), using a plasma of CHF₃, an etchant that is known to have a good selectivity between oxides and silicon;

(vi) removal of minute amounts of fluorocarbon polymers that might have formed on the etched surface during the CHF₃/RIE step (for that, use of a descum process with an oxygen plasma);

(vii) photoresist stripping;

(viii) immersing the wafer in H₃PO₄ solution (VLSI grade, 85%, 45 °C, 30 s) to remove any aluminum that might have been deposited during the RIE process;

(ix) chemisorbing OTS on the well-defined alternating stripes of titanium dioxide and (the native oxide of) silicon.

The patterned structures were characterized routinely during the preparation process by optical microscopy (Olympus BX60), to ensure the good quality of the pattern-transfer process. The width of the titanium dioxide domains and that of the silicon domains were measured at the end of the process by a Vickers Instrument M41 measuring system. The depth of the stripes was measured by profilometry (alpha-step 500, Tencor Inc.) at the end of the process, to ensure complete etching of the titanium dioxide at the unprotected areas and to measure the corrugation

of each of the domain types. The titanium dioxide films' depth profile was characterized by argon sputtering assisted Auger spectroscopy, to ensure that no other phases (such as titanium silicides) were formed at the interface between the silicon substrate and the titanium dioxide film. The same technique was used on the etched domains, to ensure the completeness of the etching step and to validate the absence of contaminants on the surface, which could have formed during the RIE process.

Since OTS molecules chemisorb on both titanium dioxide and (the native oxide of) silicon, any IR spectrum of B-type samples taken with a macroscopic size beam includes signals averaged over many silicon and titanium dioxide microstrips. Hence, we had to assume that the ratio between the number of OTS molecules on silicon domains and the number of molecules on titanium dioxide domains is equal to the ratio obtained from comparing the nonpatterned A-type samples, i.e., 1:4. This ratio was confirmed independently by micro-FTIR measurements of single stripes in B-type samples containing 40 μm width structures.

C-Type Samples. Similar to the B-type samples, the C-type structures consisted of SAMs attached to substrates made of silicon/titanium microstrips. However, unlike the B-type samples, the OTS molecules in the C-type samples were chemisorbed only on the silicon stripes, at well-defined distances from the TiO₂/Si interfaces, in a manner that the loci of the centers of the OTS stripes coincided with the centers of the silicon stripes. These samples are marked in this manuscript as "C-type (x, y, z)", where x represents the width of the titanium dioxide stripes, y represents the width of the silicon stripes, and z represents the width of the OTS stripes on the silicon domain.

The first step in the preparation of C-type samples was the preparation of OTS covered B-type structures. Then, the wafers were spin-coated with a 1.8 μm layer of a positive photoresist (AZ1818) that, after patterning by photolithography, served to protect a well-defined area on the silicon stripes, during a subsequent O₂ plasma-ashing of the monolayer in the exposed domains. To ensure complete removal of the monolayers (20 Å in thickness) at the nonprotected domains, an exposure time of 120 s was used, approximately 100 times larger than the time needed for such a thickness. Stripping of the photoresist was then done by washing with acetone, followed by immersing in a commercial stripping solution (methyl dipropylidynone, 25 °C, 30 min) and further cleaning by washing with hot chloroform and then deionized water. To ensure that the surface, obtained after the photoresist stripping, consisted of SAMs attached only to the selected areas, microprobe FTIR measurements were taken at selected domains, prior to the photoresist coating and after photoresist stripping.

2.b. Photodegradation Measurements. The kinetics of the photodegradation of the OTS monolayers on the various types of samples were measured in situ by FTIR spectroscopy in a direct absorption mode. Since during the deposition of the OTS layers both sides of the samples of the wafers were coated, care was taken to strip the backside of the wafers prior to performing the photodegradation measurements. To ensure that the front side was not damaged during the stripping of the backside, the FTIR signal of silicon wafers covered with OTS on both sides was taken prior to and after the backside stripping. The integrated absorbance following the back stripping was approximately half of the integrated absorbance measured prior to the back stripping, demonstrating the perfect stripping of the back without damaging the OTS on the front side.

To perform the photodegradation experiments, a specially built temperature and humidity controlled accessory, which

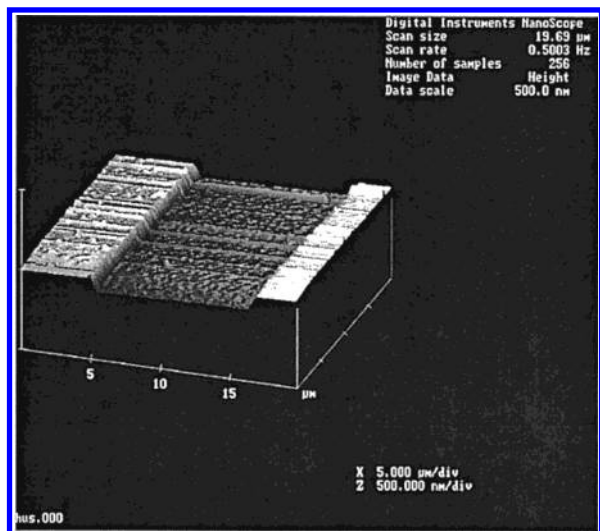


Figure 3. AFM image of a 10 μm width B-type sample.

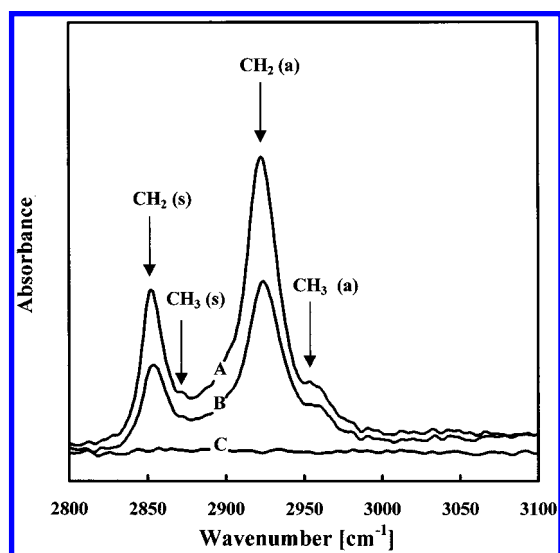


Figure 4. FTIR direct absorption spectra of OTS on a 10 μm B-type sample (surface temperature = 70 $^{\circ}\text{C}$), prior to (trace A) and after 6 min (trace B) and 68 min (trace C) of exposure to the UV light.

included also a UV (254 nm) pencil lamp was introduced into the sample compartment of the FTIR machine. The illumination power at the wafers' surface was measured by a Spectroline radiometer and was found to be 0.09 mW cm^{-2} . Unless otherwise stated, all measurements were carried out at a relative humidity of 8% and a constant surface temperature of 40 $^{\circ}\text{C}$.

3. Results

Figure 4 presents the C–H stretch envelope in the spectrum of a B-type sample made of OTS, chemisorbed on an hybrid structure of 10 μm width silicon stripes and 10 μm width titanium dioxide stripes. Note the difference between the spectrum measured prior to the UV exposure (trace A) and after 6 min of exposure (trace B). Of special interest is trace C, which shows the total disappearance of the signal following 68 min of exposure. In contrast, OTS films on nonhybrid silicon wafers did not reveal any deterioration following exposure to the UV light under the same conditions, verifying that the presence of titanium dioxide was a prerequisite for this degradation process to happen.

Figure 5 presents the integrated IR absorbance signal of the C–H stretch envelope of four B-type samples as a function of

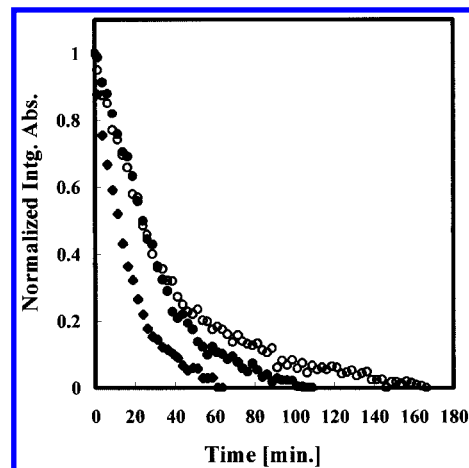


Figure 5. Decrease in the normalized integrated absorption of the C–H stretch envelope of OTS as a function of the UV exposure time, for a nonhybrid, A-type sample (\blacklozenge) and for Si/TiO₂ hybrid surfaces (B-type samples) having domain sizes of 10 μm (\bullet) and 40 μm (\circ).

exposure time, for an A-type sample, and 10 μm width and 40 μm width B-type samples. To correct for small deviations in the measured signal prior to the exposure, due to small deviations in preparation of the monolayers, the presented data was normalized with respect to the integrated absorbance at time zero. As presented in the figure, for all domain sizes the signal eventually dropped to nil. There was a distinct difference between the time needed to complete the photodegradation process of the OTS monolayer on the nonpatterned surface (60 min) and the time needed for the hybrid systems, which was larger, yet within the same order of magnitude. The larger the domain size was, the larger was the time needed to obtain complete mineralization. For example, 2.5 μm features (not shown in the figure) required 80 min, while 10 μm required 105 min and 40 μm features required as much as 165 min. This difference in the degradation rate was noticed not only during the late stages of the degradation but (to a lesser extent) also at short times.

Since OTS chemisorbed on the silicon domains accounts for approximately 20% of the total integrated absorbance measured prior to exposure, the fact that the signal dropped to zero can be explained only if OTS molecules that were on the silicon domains were photodegraded as well. The observed trend in the time required for complete mineralization versus the domain size supports this conclusion, since otherwise it could have been expected that the photodegradation kinetics would be the same for all domain sizes. The diffusion of OTS on the surface is impossible due to the chain-to-surface and chain-to-chain chemical cross-linking; hence, one must conclude that the oxidizing species were able, under the above-mentioned conditions, to reach the OTS chains on the silicon and attack them.

Figure 6 demonstrates the effect of variations in the relative humidity on the photodegradation of OTS on B-type samples, having 5 μm stripes. As can be observed in the figure, increasing the relative humidity tends to decrease the time required for the complete disappearance of the IR signal. For example, at 0% relative humidity more than a 100 min of exposure was needed, whereas at a relative humidity of 20% and 60% the required exposure time was only 60 and 40 min, respectively.

In principle, the "remote degradation phenomena" described above could be explained by one, or more, of the following mechanisms: (1) direct oxidation by charge carriers migrating from the titanium dioxide domains, where they were formed, to the silicon stripes; (2) a radical chain mechanism that

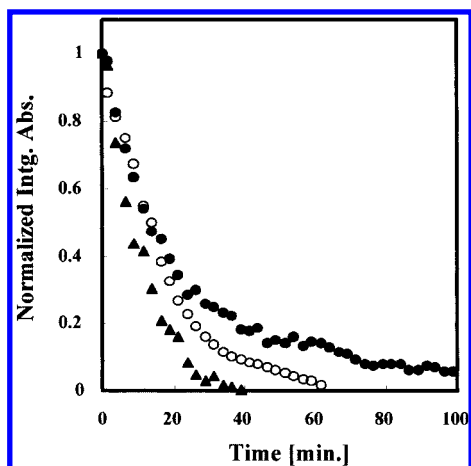


Figure 6. Photodegradation kinetics of OTS in three 5 μm B-type samples (surface temperature = 40 $^{\circ}\text{C}$), exposed to UV light under different relative humidity environments: (a) 0% RH (\bullet); (b) 20% RH (\circ); (c) 60% RH (\blacktriangle).

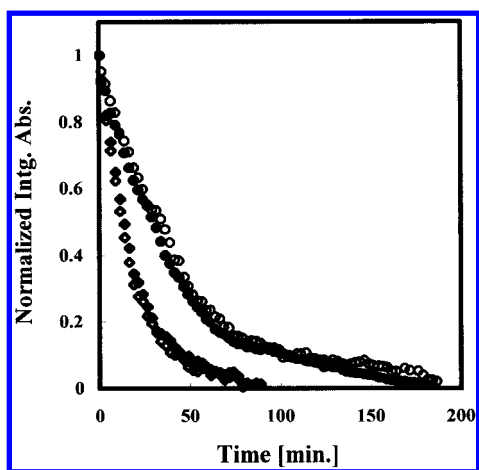


Figure 7. Photodegradation kinetics of OTS, chemisorbed on hybrid structures made of titanium dioxide and either the native oxide of silicon (empty symbols) or a thick layer of silicon oxide (filled symbols). Circles represent structures of 40 μm in width, whereas diamonds represent structures of 2.5 μm in width.

propagates from the titanium dioxide stripes to the silicon domain, by virtue of the extremely short distance between adjacent chains; (3) diffusion of oxidizing species through air; (4) surface-diffusion of oxidizing species.

To investigate the validity of mechanism 1, a new set of B-type samples was prepared. In this set, a thick (100 nm), nonconductive layer of silicon dioxide was grown on the silicon wafers by thermal oxidation prior to their coating with titanium dioxide. The photodegradation kinetics of OTS chemisorbed on this thick, nonconductive layer was compared with that of OTS on the "normal" B-type samples, where, at the silicon domains, the monolayer was chemisorbed on the ultrathin (2–4 nm) native oxide of the wafer. As demonstrated in Figure 7, the kinetics on both types were found to be exactly the same. Likewise, no difference could be found between the photodegradation kinetics of OTS on B-type samples that were prepared from N-type silicon wafers and the kinetics measured on B-type samples that were prepared from P-type silicon wafers. If the photodegradation on the silicon domains was due to a direct attack by electrons or holes, one could have expected its kinetics to depend on the substrate type (P-type, N-type, or nonconductive). Hence, the observation that the photodegradation kinetics was independent of the substrate proves that the photodegra-

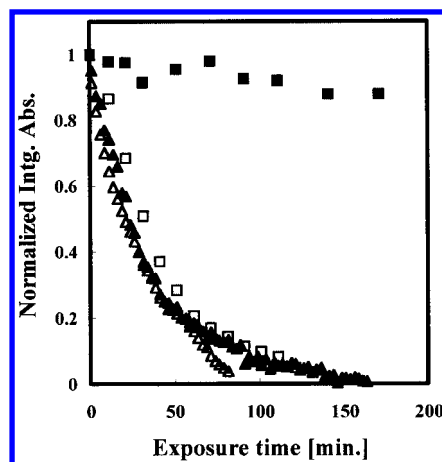


Figure 8. Comparison between the degradation kinetics of OTS on (A) back-illuminated titania-coated silica (\triangle), (B) B(40) sample (\blacktriangle), (C) C(40,40,20) sample (\square), and (D) a silicon wafer spaced 15 μm away from a back-illuminated titania-coated silica (\blacksquare).

dation on the silicon domains was not due to a direct attack by electrons or holes.

A chain propagation mechanism (mechanism 2) is characterized by an attack of the oxidizing species on an OTS molecule that is chemisorbed at a TiO_2 domain, thus creating an alkyl radical, still attached to the surface. The alkyl radical may attack an adjacent chain, and in that manner the degradation reaction may propagate into the silicon stripes. Such a mechanism was suggested in the past for the photocatalytic degradation of trichloroethylene (TCE) in air, where photoefficiencies greater than unity have been observed.¹³ Another example is the aqueous phase photodegradation of ethanol, where it was claimed that an organoperoxy radical formed by a reaction between an ethanol radical and an oxygen molecule attacks a molecule of ethanol.¹⁴ For the described above B-type samples, where the contaminants are anchored to the surface, inducing of remote degradation by a radical-chain propagation mechanism requires a very close proximity between the reacting OTS molecules at the two sides of the titania/silicon interface. A comparison between the kinetics on C-type samples and on B-type samples having TiO_2 stripes and Si stripes of the same width [C(40,40,20) versus B(40)] is presented in Figure 8. Both samples had silicon domains of 40 μm in width; however, unlike the all-covered B-type sample, the C-type sample had OTS molecules only around the center of its silicon domain, in a manner that the OTS molecules were separated by 10 μm from the titania–silicon interface. Both samples were exposed under the same conditions, i.e., a surface temperature of 40 $^{\circ}\text{C}$ and a relative humidity of 8%. As presented in the figure, the exposure time needed for a complete photodegradation of OTS in the C-type sample is ≈ 150 min, similar to the time required for the B-type sample. Nevertheless, during short illumination times, a marked difference in the kinetics was noticed, the degradation on the B-type sample being moderately faster than that on the C-type sample. The same type of behavior repeated itself with other couples of C-type and B-type samples. The difference in the kinetics at the short exposure times can be explained by the fact that during this time most of the molecules that are consumed in the B-type sample are located on TiO_2 domains, whereas molecules that are consumed on the C-type sample are located on the silicon stripes, away from the oxidizing species producing titanium dioxide domains. In contrast, the long-times kinetics represents the degradation of molecules located on the silicon domains in both types of samples. Hence, the existing of a severe obstacle for the propagation in the C-type sample

should manifest itself in the degradation rate measured at these times. The fact that the time required for a complete mineralization of the C-type sample was similar to the time required for a complete mineralization of the B-type sample indicates that the 10 μm gap existing in the C(40,40,20) sample between chains on the titanium dioxide domains and chains on the silicon domain had no significant effect on the degradation kinetics. Hence, it can be concluded that the chain propagation mechanism does not play an important role in the remote degradation phenomena.

The feasibility of remote photocatalysis by a through-air diffusion of oxidizing species was recently demonstrated in the photocatalytic bleaching of methylene blue.¹⁵ To understand the role of a through-air diffusion mechanism in the remote degradation of the OTS molecules, an experimental setup similar to the one used in the methylene blue experiments was constructed. It consisted of a 1 in. fused silica disk, coated, as previously described, with a thin layer of titanium dioxide. An OTS monolayer was chemisorbed onto another 1 in. wafer made of silicon, and the two disks were clamped together, separated by a 15 μm Teflon spacer, the OTS facing the TiO_2 layer. In the experiments, the degradation of the OTS monolayer was measured, following exposure of the titanium dioxide film to UV light that penetrated through the fused silica. To prevent the possibility of lack of humidity or oxygen in the reaction cell during the exposure, the UV light was turned off occasionally and the cell was exposed to air under the predetermined humidity conditions.

Trace D in Figure 8 presents the photodegradation kinetics in this experiment, while trace C presents, as mentioned before, the photodegradation kinetics of a C(40,40,20) sample. In this C-type sample, the distance between the TiO_2 /silicon interface and the OTS molecules is between 10 and 20 μm ; hence, the diffusion lengths in both samples are comparable. As presented in the figure, the degradation of the OTS in the C-type sample was by far faster than the degradation in the monolayer that was on the silicon in the titania-air-OTS (TAO) accessory. For example, a total disappearance of the OTS signal in the C-type sample was observed within 130 min, whereas at this time no more than 10% of the OTS in the TAO accessory was photodegraded. Same comparatively slow degradation was found also at other conditions of humidity and photon flux. They demonstrate that a through-air diffusion mechanism plays, at most, only a minor role in the remote degradation observed in the B-type and C-type samples. This conclusion is farther strengthened if one considers geometrical effects manifested by the cosine law distribution known for desorption of molecules from surfaces.

Due to the high absorption coefficient of TiO_2 at 254 nm, the charge carriers formed in the TAO experiments were generated in the bulk of the TiO_2 , mostly near the titania-silica interface, i.e., some 60–70 nm away from the titania-air interface. Hence, one might argue that the slow photodegradation kinetics in the TAO experiments was due to excessive recombination of the charge carriers in the bulk of the TiO_2 such that any comparison with the C-type samples measurements might not be valid. To verify that bulk recombination was not the reason for the slow photodegradation, measurements were taken with OTS chemisorbed on a TiO_2 -coated silica that was back-illuminated. As demonstrated in Figure 8 (trace A), back-illumination of OTS on TiO_2 film coated on fused silica yielded practically the same kinetics observed for the C-type and the B-type samples. This clearly proves that the slow photodegra-

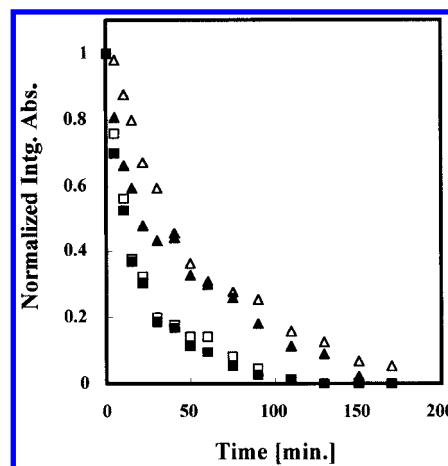


Figure 9. Photodegradation kinetics of OTS on a 40 μm width B-type sample, as measured by a microprobe FTIR. The four graphs represent 4 different subdomains: (I) TiO_2 substrate, 10–20 μm from the TiO_2 –Si interface (\square); (II) TiO_2 substrate, 0–10 μm from the TiO_2 –Si interface (\blacksquare); (III) silicon substrate, 0–10 μm from the TiO_2 –Si interface (\blacktriangle); (IV) silicon substrate, 10–20 μm from the TiO_2 –Si interface (\triangle).

dation kinetics in the TAO experiments had nothing to do with the fact that the thin TiO_2 film was back-illuminated.

The data that were presented so far on the B-type samples were collected by measuring the OTS signal on a large ensemble of stripes, in a manner that could not differentiate between OTS on the silicon domains and OTS on the titanium dioxide domains. To differentiate between the reaction kinetics of molecules anchored to the titanium dioxide and molecules attached to the silicon surface, the reaction kinetics on a 40 μm silicon stripe and on its adjacent 40 μm titanium dioxide stripe were measured separately. For these measurements, a microprobe accessory (Bruker) allowing the measuring of a measured stripe of 10 μm by 570 μm was used. Obviously, the 9000 \times reduction in the spot area had its toll on the signal-to-noise (s/n) ratio; still a reasonable s/n ratio could be achieved by a long-time (15 min) averaging.

The degradation kinetics on a single stripe of titanium dioxide and on its adjacent silicon stripe is presented in Figure 9. The figure shows the photodegradation kinetics at 4 distinct areas: (I) TiO_2 substrate, 10–20 μm from the TiO_2 –Si interface; (II) TiO_2 substrate, 0–10 μm from the TiO_2 –Si interface; (III) silicon substrate, 0–10 μm from the TiO_2 –Si interface; (IV) silicon substrate, 10–20 μm from the TiO_2 –Si interface. Each point represents an average of three different locations on the wafer. The figure clearly shows a decrease to nil in the signal in all the subdomains. A comparison between the photodegradation kinetics on the silicon domain and on the titanium dioxide domain reveals that the kinetics on the silicon were slower than the kinetics on the TiO_2 , as could have been expected. Nevertheless, the degradation of the OTS on the silicon begins immediately upon exposure and there is no lag time between subdomains II and III. The kinetics on the two TiO_2 subdomains were found to be almost identical, whereas on the Si subdomains a noticeable difference in the kinetics between the two subdomains could be observed. Here, degradation kinetics on subdomain III, which was closer to the TiO_2 domain II, was found to be faster than degradation kinetics on subdomain IV, in particular during the first 30 min of exposure. It is noteworthy that, prior to UV illumination, the amount of OTS measured by the microprobe on the titanium dioxide domains was approximately four times higher than on the silicon domains, in line with our previous calculations, that were based, as

mentioned in the Experimental and Methods Section, on comparing between signals obtained from A-type, nonhybrid surfaces.

4. Discussion

The presented data proves that remote photodegradation can occur in molecules anchored at the vicinity of titanium dioxide microdomains. It further provides a hint on the mechanism by elucidating that this remote photodegradation is mainly due to surface migration of active species which are not electrons or holes. These species seem to diffuse a relatively large distance before reacting, in certain cases up to 20–40 μm . Furthermore, the diffusion coefficient seems to be high enough to cause remote destruction even at very short times, as inferred from the microprobe measurements.

To get a better insight on the remote degradation phenomena, the kinetics of the photodegradation of OTS on A-type and B-type samples was measured at four surface temperatures (303, 313, 343, and 383 K). At all temperatures, the kinetics of the A-type samples could be fitted easily (confidence parameter > 0.96) to exponentially decaying curves $I = \exp[-F_{0,T}t]$, suggesting apparent first-order kinetics. Here, I is the normalized integrated absorbance, $F_{0,T}$ is a temperature-dependent fitted parameter, and t is the time (min). Plotting the logarithm of the reaction constant versus the reciprocal of the temperature yielded a straight line, with a confidence parameter of 0.95. From its slope, an apparent activation energy of 0.24 eV was calculated.

Going over the literature, one finds cases where, at the technologically relevant temperature range, the dependence on the temperature was of an Arrhenius type,¹⁶ together with cases having a linearly increasing dependency¹⁷ or even cases where increasing the temperature reduced the photodegradation rate.¹⁸ Therefore, it is noteworthy that unlike other systems where the effect of temperature on photodegradation kinetics may reflect a competition between adsorption and reaction, the photodegradation in the present experiments reflects only reaction kinetics. Although we could not find in the literature any data on the activation energy of homologue molecules that were photocatalytically degraded, it might be of interest to compare the obtained value of 0.24 eV with that of 0.22 eV for butanol,¹⁹ 0.11 eV for salicylic acid,²⁰ or 0.134 eV for oxalic acid.²¹

An exponentially decaying curve was fitted also to the kinetics measured at surface temperature of 313 K at different relative humidity. Here, $F_{0,313}$ was found to moderately depend on the relative humidity, increasing from 0.072 at 0% RH to 0.11 at 40% RH.

In contrast to the A-type samples, the degradation kinetics of the B-type samples could not be fitted to a single exponentially decaying curve. The observation that the photodegradation on both types of domains (titania and silicon) begins immediately upon exposure (Figure 9) provided a rationale for a biexponential decaying curve (Figure 10A):

$$I = J \exp[-F_{W,T}t] + (1 - J) \exp(-G_{W,T}t) \quad (1)$$

Here $\exp(-F_{W,T}t)$ represented a fast decaying component, related to photodegradation on titanium dioxide domains of width W and surface temperature T , and $\exp(-G_{W,T}t)$ represented a slow component related to photodegradation on the silicon stripes. Accordingly, the preexponential factors J and $(1 - J)$ reflected the relative contribution of OTS molecules on titania and on silicon, respectively, to the IR signal. For all stripes' width and all the measured surface temperatures, a J value of 0.75 ± 0.05 was obtained, very similar to the value of

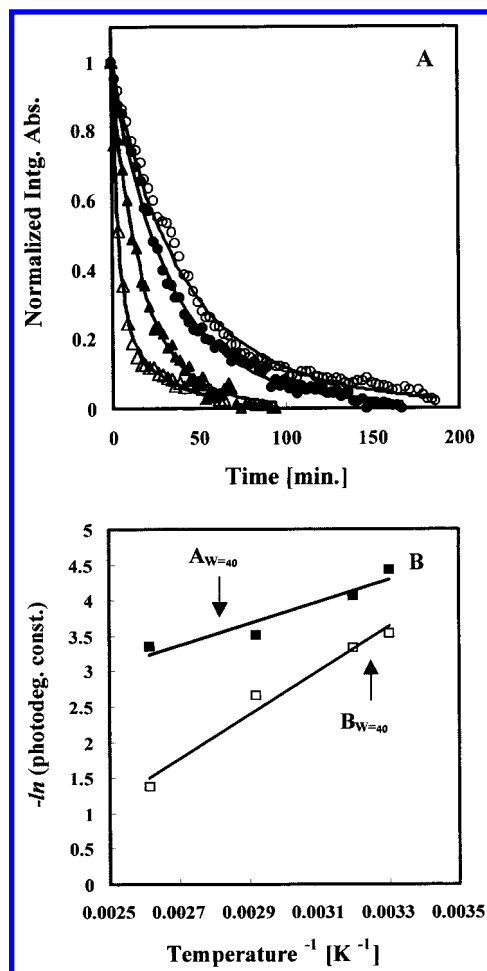


Figure 10. (A) Biexponential fitting of the photodegradation kinetics of OTS on 40 μm width B-type samples at various surface temperatures: 303 K (○); 313 K (●); 343 K (▲); 383 K (△). (B) Arrhenius plot of the two photodegradation constants $F_{40,T}$ (■) and $G_{40,T}$ (□).

0.8 ± 0.05 that was obtained from the FTIR-microprobe measurements and from measurements with A-type samples (see Experimental and Methods Section for details).

Plotting the logarithm of the photodegradation coefficients $F_{W,T}$ and $G_{W,T}$ versus the reciprocal temperature (Figure 10B) gave two distinct apparent activation energies, E_{af} and E_{ag} , respectively. Although $F_{W,T}$ and $G_{W,T}$ were found to decrease upon increasing the stripes' width (W), the apparent activation energies obtained from the Arrhenius plots (E_{af} and E_{ag}) were found to be independent of the stripes' width and had values of 0.25 ± 0.01 and 0.09 ± 0.02 eV, respectively. It is noteworthy that this value of E_{af} that was calculated for the B-type samples was equal, within a small experimental error, to the activation energy found for the A-type samples.

The same biexponentially decaying function was fitted also to the kinetics of photodegradation of OTS on 4 sets of B-type samples (stripes' width = 5, 10, 20, 40 μm). In each set, measurements were taken at relative humidity values of 0%, 8%, 20%, 40%, and 60%. Here, the surface temperature was constant and equal to 313 K. Similar to the results obtained for the A-type samples, the F parameter in these measurements was found to increase very moderately with temperature. For example, the calculated value of $F_{5,313}$ was 0.065 at 0% RH and 0.094 at 60% RH. Likewise, $F_{40,313}$ was 0.055 at 0% RH and 0.073 at 60% RH. In contrast to the moderate increase found for the F parameter, the G parameter in the fit was found to depend very strongly on the relative humidity. For example,

the calculated value of $G_{5,313}$ was 0.005 at 0% RH and 0.09 at 60% RH and the calculated value of $G_{40,313}$ was 0.005 at 0% RH and 0.024 at 60% RH. Since F and G are attributed to the kinetics on the titanium dioxide and on the silicon, respectively, this difference between the behavior of photocatalytic coefficients may imply a difference between the mechanism on the silicon domains and the mechanism on the titanium dioxide domains. Such difference between the domains can be explained, for example, on the basis of a direct oxidation mechanism that does not require hydroxyl radicals and may exist on the TiO_2 domains but not on the silicon domains (see Figure 7). Indeed, it was pointed out in the past²² that direct oxidation may take place under conditions where the concentration of the contaminants is very high or when the molecules are strongly adsorbed on the surface. These two conditions exist in the A-type samples and in the TiO_2 domains of the B-type samples. Hence, such a mechanism cannot be excluded, especially under very low relative humidity and at short exposure times when the surface is fully covered with the organic molecules, thus preventing the adsorption of water.²³

The chemical species involved in the remote degradation may be hydroxyl radicals, superoxide anions, hydrogen peroxide molecules, or even singlet oxygen,²⁴ claimed to be generated on the surface of irradiated titanium dioxide. Molecular oxygen participates in the reaction at later stages, as proposed for other photocatalytic reactions in the gas phase.²⁵ Higher photodegradation rates upon increasing humidity is often regarded as, at least, supportive evidence for a hydroxyl radical mediated mechanism.²⁶ Although the surface diffusion of hydroxyl radicals for such long distances seems to contradict the general belief in the field, there is nothing in the data we present that is not in line with such a possibility.

During exposure of B-type samples half of the impinging photons are wasted, being absorbed by the silicon domains. Since in all the B-type samples the silicon stripes cover 50% of the total area, one could expect that the degradation rate in the B-type samples would be slower by at least 50%, compared with the degradation rate on the A-type samples. Since the photoefficiency in these experiments is a function of exposure time, it is possible to make such comparisons accurately only if they are based on the initial photodegradation rates. Examining the initial photodegradation rates of all the B-type samples having stripes' width of 2.5 and 5 μm revealed, in contrast to expectations, that they were slower than the rates of A-type samples exposed under the same temperature and humidity conditions by less than the expected 50%. For example, the initial rate of B-type sample having 2.5 μm width domains exposed at 30 °C and 8% RH was only 22% slower than the rate on the corresponding A-sample. Likewise, the initial rate of B-type sample having 5 μm width domains exposed at 110 °C and 8% RH was only 13% slower than the rate on the corresponding A-sample. To explain these findings, it is suggested that the silicon domains serve as a sink for the oxidizing species, thus reducing the rate of recombination reactions on the titanium dioxide domains. Indeed, such spillover phenomena²⁷ are known in the literature, mainly in systems containing hydrogen or oxygen atoms in metal/nonmetal hybrid structures. However, to the best of our knowledge, there is no conclusive documentation of spilling over of hydroxyl radicals to such distances.

5. Conclusion

It was shown that photogenerated oxidizing species, formed on titanium dioxide well-defined microdomains, are capable of

inducing, within minutes, the mineralization of aliphatic chains anchored to inert silicon domains, even when these chains are located as far as 20 μm away from the titanium dioxide microzones. The remote photodegradation effect was not due to direct oxidation by charge carriers, although such a mechanism may exist on the titanium dioxide domains, but is due to out-diffusion of oxidizing species, probably on the surface.

It is believed that these findings may have a very important effect on the designing of new photocatalytic reactors for air cleaning that may utilize the remote degradation phenomena. It is further possible that the high efficiencies found in some of the modern air-cleaning photocatalytic reactors are due to remote degradation effects in dark, yet operative, areas.

A detailed model that will take into consideration temperature and humidity effects in a more fine-tuned manner is under preparation and will be presented elsewhere.

Acknowledgment. This work was supported by the Israel Science Foundation (Grant No. 75-98-1). The authors thank T. Aqua and G. Shemer for their help.

References and Notes

- (1) For example: (a) Holmann, M. M. Photodegradation of water pollutants; CRC Press: Boca Raton, FL, 1996. (b) Blake, B. M. *Bibliography of Work on the Photocatalytic Removal of Hazardous Compounds from Water and Air*; NREL: Golden, CO, 1994. (c) Fujishima, A.; Honda, K. *Nature* **1972**, 238, 37.
- (2) Saka, T.; Kawai, T. *Chem. Phys. Lett.* **1981**, 80, 341.
- (3) Wei, C.; Lin, W. Y.; Zanal, Z.; Williams, N. E.; Zhu, K.; Krunic, A. P.; Smith, R.L.; Rajeshwar, K. *Environ. Sci. Technol.* **1994**, 28, 934.
- (4) (a) Hsiao, C.-Y.; Lee, C.-L.; Ollis, D. F. *J. Catal.* **1983**, 82, 418. (b) Matthews, R. W. *J. Phys. Chem.* **1987**, 91, 3328.
- (5) (a) Sopian, I.; Watanabe, M.; Murasawa, S.; Hashimoto, K.; Fujishima, A. *J. Photochem. Photobiol., A* **1992**, 98, 79. (b) Peral, J.; Ollis, D. F. *J. Catal.* **1992**, 136, 554.
- (6) Anderson, C.; Bard, A. J. *J. Phys. Chem.* **1995**, 99, 9882.
- (7) Takeda, N.; Ohtani, M.; Torimoto, T.; Kuwabata, S.; Yoneyama, H. *J. Phys. Chem. B* **1997**, 101, 2644.
- (8) Paz, Y.; Luo, Z.; Rabenberg, L.; Heller, A. *J. Mater. Res.* **1995**, 10, 2842.
- (9) Paz Y.; Heller A. *J. Mater. Res.* **1997**, 12, 2759.
- (10) Sagiv, J. *J. Am. Chem. Soc.* **1980**, 102, 92.
- (11) Cohen, S. R.; Naaman, R.; Sagiv J. *J. Phys. Chem.* **1986**, 90, 3054.
- (12) Zemel, E.; Haick, H.; Paz, Y. *J. Adv. Oxid. Technol.*, in press.
- (13) (a) Jacoby, W. A.; Blake, D. M.; Noble, R. D.; Koval, C. A. *J. Catal.* **1995**, 157, 87. (b) Luo, Y.; Ollis, D. F. *J. Catal.* **1996**, 163, 1. (c) Berman, E.; J. Dong, J. In *Chemical Oxidation-Technologies for the Nineties*; Eckenfelder, N. N., et al., Eds.; Nashville, TN, 1992; Vol. 3, p 183.
- (14) Ikeda, K.; Sakai, H.; Baba, R.; Hashimoto, K.; Fujishima, A. *J. Phys. Chem. B* **1997**, 101, 2617.
- (15) Tatsuma, T.; Tachibana, S.; Miwa, T.; Tryk, D. A.; Fujishima, A. *J. Phys. Chem. B* **1999**, 103, 8033.
- (16) Okamoto, K.; Yamamoto, Y.; Tanaka, H.; Itaya, A. *Bull. Chem. Soc. Jpn.* **1985**, 58, 2023.
- (17) Bahnemann, D.; Bockelmann, D.; Goslich, R. *Sol. Energy Mater.* **1991**, 24, 564.
- (18) Courbon, H.; Hermann, J.-M.; Pichat, P. *J. Catal.* **1985**, 95, 539.
- (19) Cunningham, J.; Hodnett, B. K. *J. Chem. Soc., Faraday Trans. 1* **1981**, 77, 2777.
- (20) Matthews, R. W. *J. Phys. Chem.* **1987**, 91, 3328.
- (21) Herrmann, J.-M.; Mozzanega, M.-N.; Pichat, P. *J. Photochem.* **1983**, 22, 333.
- (22) Gerischer, H.; Heller, A. *J. Phys. Chem.* **1991**, 95, 5261.
- (23) Cave, N. G.; Kinloch, A. J. *Polymer* **1992**, 33, 1161.
- (24) Dunlap, W. C.; Yamamoto, Y.; Inoue, M.; Kashiba-Iwatsuki, M.; Yamaguchi, M.; Tomita, K. *Int. J. Cosmet. Sci.* **1998**, 20, 1.
- (25) Ohko, Y.; Hashimoto, K.; Fujishima, A. *J. Phys. Chem. A* **1997**, 101, 8057.
- (26) Kawai, M.; Kawai, T.; Naito, S.; Tamaru, K. *Chem. Phys. Lett.* **1984**, 110, 58.
- (27) Conner, W. C., Jr.; Falconner, J. L. *Chem. Rev.* **1995**, 95, 759.